ORIGINAL RESEARCH ARTICLE

Effect of Sr Modification on the Microstructures, Mechanical Properties, and Thermal Conductivity of Hypoeutectic Al-13.6Cu-6Si Alloys

Chengbo Li, Huibing Hou, Leilei Liu, Chengyi Huang, Yuelu Ren, Jun Du, and Cailiu Yin

The effects of Sr modification on the microstructure, mechanical properties, and thermal conductivity of the hypoeutectic Al-13.6Cu-6Si alloy were thoroughly investigated in the past using techniques such as optical microscopy, scanning electron microscopy, x-ray diffraction, cooling curve thermal analysis (CA-CCTA), universal testing machine, and laser thermal conductivity analyzer. The findings showed that the introduction of an appropriate amount of Sr into the alloy resulted in additional undercooling, enhancing the rate of non-uniform nucleation and significantly refining the α-Al grains. Furthermore, it effectively modified the morphology of eutectic silicon phases, transforming the plate-like structure into a fine and uniform coral-like appearance. Notably, the optimal modification effect was achieved with the addition of 0.3% Sr. Compared to the alloy without Sr modification, the secondary dendrite arm spacing of α-Al in the alloy was reduced from 14.26 to 9.23 μm. Additionally, the thermal conductivity, ultimate tensile strength, and elongation were significantly of the alloy increased to 130.1 W/(m K), 322 MPa, and 4.6%, respectively, representing an improvement of 10, 19, and 53%, respectively.

1. Introduction

High thermal conductivity alloy with acceptable strength has generated widespread interest due to the rising demand for heat dissipation of electronic devices (Ref 1-4). It is necessary to search for materials that are lightweight, good processing properties, low-cost, and suitable corrosion resistance under humid environment (Ref 5-7). Undoubtedly, Al-Si alloys are excellent materials for the aforementioned applications due to their favorable mechanical properties, exceptional castability,

and cost-effectiveness (Ref 8-14). However, the relatively low thermal conductivity (e.g., the limited thermal conductivity of ADC12 is 96 W/(m K) (Ref 15)) hinders their use in electronic communication, particularly in the advanced integration of fifth-generation (5G) mobile network (Ref 16, 17). In the past few years, there has been an increasing fascination with Al-Cu-Si alloys because of their distinct performance (Ref 18-22). Numerous research studies have indicated that Al-Cu-Si alloys exhibit superior corrosion resistance in comparison with Al-Cu alloys, and they also possess greater strength than Al-Si alloys (Ref 23). Furthermore, Al-Cu-Si ternary alloys are suitable for cost-effective mass production of castings through low-cost high-pressure die casting (HPDC) methods, owing to their exceptional fluidity (Ref 24, 25). Despite this, there remains room for enhancing the thermal conductivity and mechanical characteristics of Al-Cu-Si ternary alloys. Concerning the microstructure, the presence of a flake-like eutectic Si phase adversely affects the mechanical properties and thermal conductivity of Al-Cu-Si alloys. It is widely acknowledged that these alloys tend to exhibit relatively poor tensile ductility and thermal conductivity due to this microstructural characteristic. In order to tackle this problem, the alloy undergoes Sr modification, which is a widely used technique in the industry, to improve its strength, elongation, and thermal conductivity (Ref 26-28). Previous studies have solely concentrated on improving the physical characteristics of the Al-Cu-Si alloy by means of Sr modification (Ref 29-31). However, limited studies have delved into the correlation between Sr modification and thermal conductivity properties. It is worth mentioning that morphological changes of the eutectic Si phase offer a viable strategy for enhancing both thermal conductivity and mechanical characteristics simultaneously.

The primary objective of this study is to design a high thermal conductivity Al-Cu-Si alloy while maintaining accept-

Chengbo Li, School of Materials Science and Engineering, South China University of Technology, Guangzhou 510641, China; Guangxi Key Laboratory of Materials and Processes of Aluminum Alloys, ALG Aluminum lnc., Nanning 530031, China; and Guangxi Key Laboratory of Advanced Structural Materials and Carbon Neutralization, School of Materials and Environment, Guangxi Minzu University, Nanning 530105, China; **Huibing Hou, Leilei Liu**, and **Cailiu Yin**, Guangxi Key Laboratory of Advanced Structural Materials and Carbon Neutralization, School of Materials and Environment, Guangxi Minzu University, Nanning 530105, China; **Chengyi Huang**, School of Materials Science and Engineering, South China University of Technology, Guangzhou 510641, China; and Guangxi Key Laboratory of Materials and Processes of Aluminum Alloys, ALG Aluminum lnc., Nanning 530031, China; **Yuelu Ren**, Guangxi Key Laboratory of Materials and Processes of Aluminum Alloys, ALG Aluminum lnc., Nanning 530031, China; **Jun Du**, School of Materials Science and Engineering, South China University of Technology, Guangzhou 510641, China. Contact e-mail: tandujun@sina.com.

able mechanical properties. To achieve this, the Al-Cu-Si alloy was modified using the Sr element to enhance both its thermal conductivity and tensile properties simultaneously. This study will investigate how the Sr content affects the evolution of microstructure, thermal conductivity, and mechanical properties in Al-Cu-Si eutectic alloys. Through Sr modification, valuable insights will be gained into the mechanisms that contribute to the improvement of thermal conductivity and mechanical properties. Ultimately, the goal is to offer novel process and theoretical guidance for the advancement of aluminum alloys with high thermal conductivity.

2. Materials and Methods

2.1 Preparation of Samples

Al-13.6Cu-6Si-based alloys with varying Sr contents were synthesized using commercially pure Al (99.98%, Long plate), Al-50Cu (Cast waffle), Al-20Si (Cast waffle), and Al-10Sr (Cast waffle) master alloys (mass ratio, as indicated below unless specified otherwise). The measured compositions of hypoeutectic Al-13.6Cu-6Si-xSr (x = 0.1%, 0.3%, 0.5%) alloys are shown in Table 1. To begin with, aluminum ingots were melted at 750 °Cin the graphite clay crucible by electric resistance furnace. Following that, the Al-50Cu and Al-20Si master alloys were added in order to produce the Al-13.6Cu-6Si alloy. To achieve thorough homogenization, the liquid metal was agitated with a magnesium oxide rod for about 5 minutes. After modifying the Al-13.6Cu-6Si alloy by adding different amounts of Al-10Sr master alloy, the molten alloys were poured into a preheated steel mold at 200 °C, forming rectangular alloy ingots with dimensions of 100 mm × 60 mm × 15 mm. It is important to note that the Al-13.6Cu-6Si alloy without Sr modification is referred to as the "Sr-free alloy," while the alloys with Sr addition are termed "Sr-containing alloys." The cooling rate observed during the process of solidification was around 35 °C/s. Electrical discharge machining (EDM) was used to machine the as-cast alloy ingots into samples for tensile and thermal conductivity testing.

2.2 Measurements

In order to examine the microstructure of the alloys, the utilization of optical microscopy (OM) with a Leica DMI3000 microscope and scanning electron microscopy (SEM) with a JEOL JSM-6610A microscope operating at 20 kV was implemented. The alloys' phase composition was determined by employing energy-dispersive x-ray spectroscopy (EDS) through the Oxford x-Max system. Furthermore, x-ray diffraction (XRD) analysis was conducted using a Bruker D8

Advance device that had a Cu-Kα radiation source (λKα = 0.154 nm) and a scanning speed of 5°/min. An Instron 5982 testing machine was utilized to perform the tensile tests at room temperature, employing a strain rate of 0.5 mm/min. For the purpose of thermal analysis, a computer-assisted technique called cooling curve thermal analysis (CA-CCTA) was utilized. This involved continuously recording the temperature–time data of the melts using a K-type thermocouple. To guarantee the consistency of the experimental outcomes, the thermal examination of every alloy was repeated a minimum of three times using the NI 9212 rapid data acquisition system, connected to a computer operating LabView 2015, to record data at a dynamic frequency of 80 Hz/ch.

In order to determine the thermal diffusivity, disks with dimensions of $\varphi 12.7 \times 3$ mm^2 were created from the as-cast Al-13.6Cu-6Si-xSr alloys for measurement purposes. Thermal diffusivity was measured at ambient temperature (20 °C) using a Netzsch LFA457 apparatus employing the laser flash method. The Archimedes method was employed to determine the sample densities, while the Neumann–Kopp rule was utilized to calculate the specific heat capacities of the Al-13.6Cu-6Si-xSr alloys (Ref 32-34). Thus, the thermal conductivity (λ) can be determined by utilizing the subsequent equation.

$$\lambda = \alpha \cdot \rho \cdot C_p \qquad \text{(Eq 1)}$$

In the formula, α denotes the thermal diffusivity (cm^2/s), ρ represents the density (g/cm^3), and C_p stands for the specific heat capacity (J/(g K)). The estimated uncertainty for the thermal conductivity was below 5%. In order to guarantee the replicability of the experiment, three repetitions were conducted for each sample in every test. The mean was subsequently computed based on these various measurements. This approach helps to minimize potential errors or variations in the experimental results. Furthermore, the sample's conductivity was evaluated at room temperature (20 °C) using eddy current technology (PZ-60A). To ensure data accuracy, 10 measurement points were uniformly selected on both sides of the sample, and their average value was calculated.

3. Results and Discussion

3.1 Microstructure

Figure 1 illustrates the typical microstructures of as-cast Al-13.6Cu-6Si alloys with varying Sr contents. Figure 1a shows that the microstructure of the Al-13.6Cu-6Si alloy in its as-cast state is composed of dendritic α-Al, a large plate-like eutectic Si phase, and a continuous reticulated Al$_2$Cu phase. Image Pro Plus software was utilized to determine the secondary dendrite

Table 1 The measured compositions of hypoeutectic Al-Cu-Si alloys with varied Sr contents

Alloy name	Cu	Si	Sr	Fe	Mg	Others	Al
	Alloy compositions, wt.%						
Al-13.6Cu-6Si	13.49	6.05	…	0.04	0.02	< 0.01	Bal
Al-13.6Cu-6Si-0.1Sr	13.58	5.99	0.09	0.03	0.03	< 0.01	Bal
Al-13.6Cu-6Si-0.3Sr	13.66	5.97	0.32	0.05	0.02	< 0.01	Bal
Al-13.6Cu-6Si-0.5Sr	13.56	6.13	0.46	0.04	0.01	< 0.01	Bal

arm spacing (SDAS) of α-Al. For the Sr-free alloy, the (SDAS) value was approximately 14.26 μm. As Fig. 1(b-d) demonstrates, there is a notable difference in microstructure upon the addition of Sr. The introduction of Sr leads to a refined and more uniform dendritic α-Al structure. With the increase in Sr content to 0.3%, the SDAS value experiences a gradual decrease from 14.26 to 9.23 μm, which proves advantageous in improving mechanical characteristics. However, when the Sr content is further elevated to 0.5%, the secondary dendrites become coarser and the SDAS value rises to 11.95 μm.

Moreover, the presence of Sr in the Al-13.6Cu-6Si alloy results in a metamorphosis of the eutectic Si phase, causing it to transition from a coarse slab to a comparatively delicate slab or coral-like formation. These discoveries suggest that Sr exerts a substantial transformative influence on the eutectic Si phase. These findings indicate that Sr has a notable modifying influence on the eutectic Si phase. Nevertheless, when the Sr content rises to 0.5%, the influence of Sr on modification appears to decrease. There are no significant morphological differences observed in the reticulated Al$_2$Cu phase between Sr-free and Sr-containing alloys. In conclusion, the findings mentioned above indicate that the optimal microstructure is attained when the Sr content in the Al-13.6Cu-6Si alloy is 0.3%.

Figure 2a displays the XRD patterns, indicating that the Al-13.6Cu-6Si alloys, whether Sr-free or Sr-containing, comprise α-Al, Al$_2$Cu, and Si phases. However, due to the low amount of Sr added, it is difficult to identify any Sr-bearing intermetallic compounds. An enlarged perspective of the most prominent peak in the α-Al phase is shown in Fig. 2b. Notably, the diffraction peak shifts toward the left and approaches the standard diffraction peak of pure Al (as depicted by the red dotted line in Fig. 2b). The presence of the Al2Si2Sr phase (Ref 28, 29) and Al8Si15Sr4 phase may contribute to this phe-nomenon, leading to a decrease in the silicon solid solution and purification of the α-Al matrix. Consequently, the addition of Sr diminishes lattice distortion and enhances the thermal conductivity of hypoeutectic Al-13.6Cu-6Si alloy.

Figure 3 illustrates the SEM morphologies of the as-cast Sr-free and Sr-containing alloys. The x-ray diffraction (XRD) and energy-dispersive x-ray spectroscopy (EDS) findings validate that the black matrix, plate-like black phase, and continuous network white phase observed in the Sr-free alloy correspond to the existence of α-Al, Si, and Al$_2$Cu, respectively. In the Sr-free alloy, the eutectic Si phase is mainly distributed along the grain boundary, with a length varying from 20 to 45 μm (as seen in Fig. 3a and identified as Point B). The addition of 0.1% Sr effectively reduces the length of the Si phase to 15-25 μm (see specifics in Fig. 3b and Point C). When the Sr content reaches 0.3%, the Si phase experiences a change in its morphology, transitioning from a rough plate-like form to a delicate and consistent coral-like structure (refer to details in Fig. 3c and Point E). When the Sr content reaches 0.5%, although the number of coral-like Si phases in the alloy increases, a small amount of plate-like Si phases reappear, and their volume is much higher than that of coral-like Si phases (see details in Fig. 3d). Figure 3(e-h) displays the mapping outcomes of EDS. The observation indicates that the Copper element not just forms the Al$_2$Cu phase at the grain boundary but also dissolves within the α-Al matrix (refer to details in Fig. 3f). Significantly, the spatial arrangement of Sr bears a striking resemblance to that of Si, suggesting that Sr atoms adhere to the surface where Si grows, aiding in the creation of Si twins (Ref 35-37). Furthermore, the inclusion of Sr element has negligible influence on the shape and dispersion of the Al$_2$Cu phase (refer to Fig. 3(a-d) for more information).

In Fig. 4a, the solidification curves and the corresponding first derivative curves of Al-13.6Cu-6Si and Al-13.6Cu-6Si-
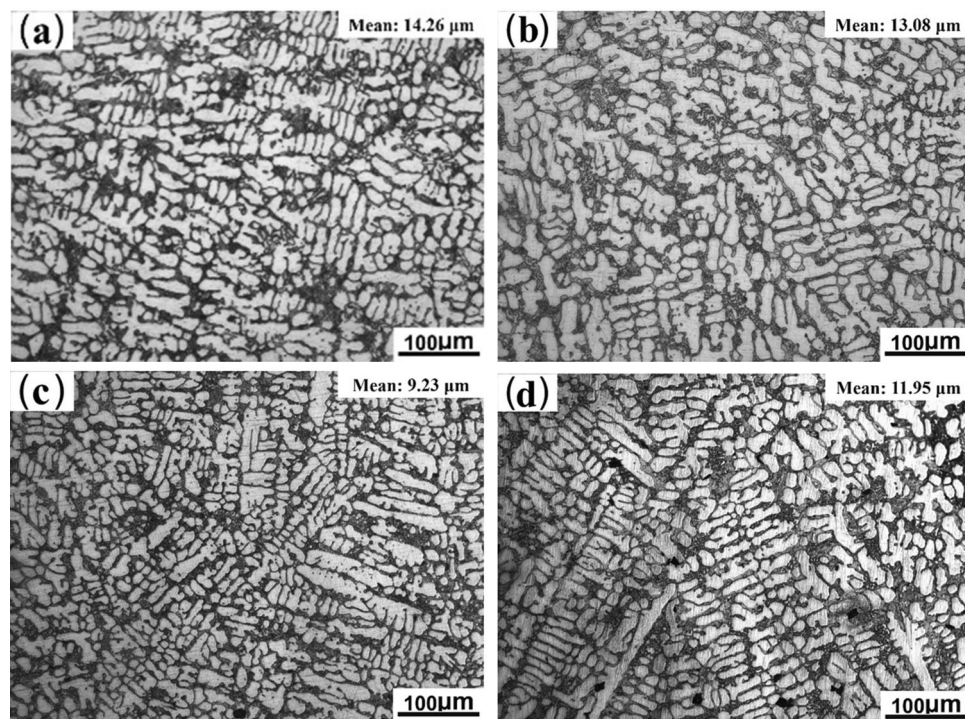

Fig. 1 The microstructures of as-cast Al-13.6Cu-6Si alloys with various Sr contents: (a) Sr-free alloy; (b) alloy with 0.1% Sr; (c) alloy with 0.3% Sr; (d) alloy with 0.5% Sr
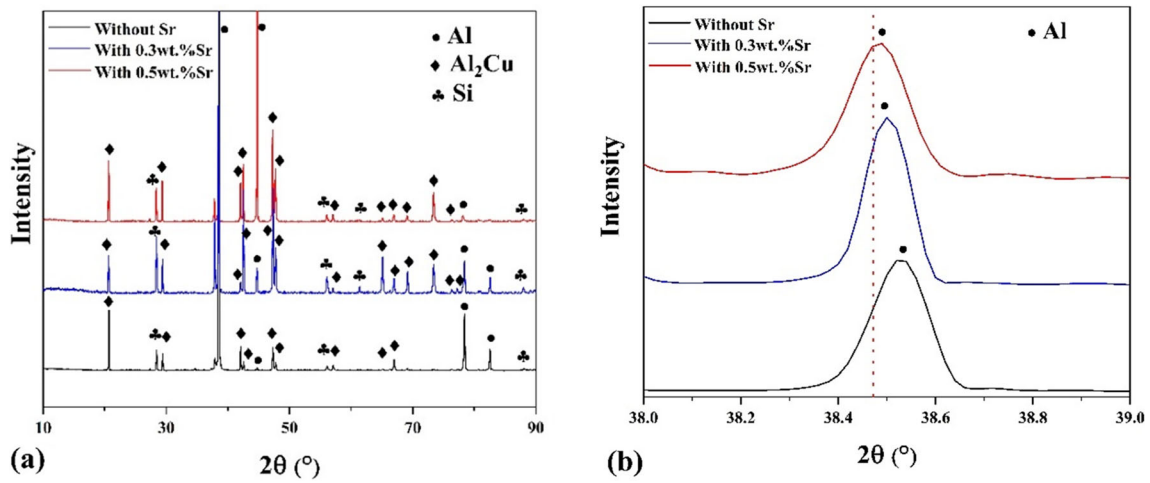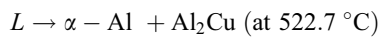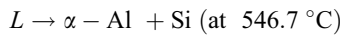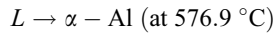
Fig. 2 (a) XRD patterns of the Sr-free and Sr-containing Al-13.6Cu-6Si alloys, (b) magnified XRD spectra in the angular range of 38°-39°

0.3Sr melts are depicted. Figure 4(b-d) illustrates enlarged pictures of the α-Al, Al-Si eutectic composition, and Al-Al$_2$Cu eutectic composition. Table 2 presents the solidification characteristic parameters of phase transformation for the examined alloys. Furthermore, Table 3 displays the solidification characteristics of the α-Al, Al-Si, and Al-Al$_2$Cu eutectic phases obtained from the solidification curves.

Figure 4a displays three peaks, each linked to distinct phase reactions in the Al-13.6 Cu-6Si alloy. In order to further examine the alloy's solidification path, JmatPro software was utilized, and Fig. 5 shows the obtained outcomes. The computed results reveal three phase reactions occurring throughout the solidification procedure, as outlined below.

$$L \rightarrow \alpha - \text{Al (at 576.9 °C)}$$

$$L \rightarrow \alpha - \text{Al} + \text{Si (at 546.7 °C)}$$

$$L \rightarrow \alpha - \text{Al} + \text{Al}_2\text{Cu (at 522.7 °C)}$$

According to the forecasted solidification path of the base alloy by JmatPro (Fig. 5), it can be inferred that the initial peak signifies the formation of the primary α-Al phase. The subsequent peak represents the eutectic reaction of Al-Si, and the final phase reaction is the formation of the Al-Al$_2$Cu eutectic structure. These phase evolutions are also observed in the Al-13.6Cu-6Si alloy containing 0.3% Sr in the present work. Furthermore, it is apparent from the curves in Fig. 4(b-d) that the cooling behavior associated with the reaction areas of α-Al, Al-Si, and Al-Al$_2$Cu phases is influenced by the addition of Sr. The variations of the solidification parameters are determined for the investigated alloys shown in Table 3.

The characteristic parameters of α-Al, obtained from the recorded solidification curves and first derivative curves, are displayed in Table 3. As for the based alloy, the temperatures for the α-Al phases, denoted as $T_n^{\alpha-\text{Al}}$, $T_{\text{Min}}^{\alpha-\text{Al}}$, and $T_G^{\alpha-\text{Al}}$ are 571.6, 569.2, and 570.9 °C, correspondingly. It is worthy to mention that the Sr addition decreases the above parameters at the same time. In the context of heterogeneous nucleation, the nucleation rate (N) can be formulated as:

$$N = f_1 C_1 \exp\left(\frac{Af(\theta)}{\Delta T^2}\right) \quad \text{(Eq 2)}$$

$$f(\theta) = \frac{2 - 3\cos\theta + \cos^3\theta}{4} \quad \text{(Eq 3)}$$

The value of f_1 represents the rate at which atoms are transferred from the liquid phase to the solid crystal nucleus. C_1 represents the density of atoms in the liquid that come into contact with regions of heterogeneous nucleation per unit volume. θ represents the angle of contact between the solid phase and the substrate for nucleation. A is the area between solid phase and nucleation substrate. ΔT is the undercooling for nucleation. Based on the above equation, we can understand that the greater the undercooling, the greater the heterogeneous nucleation rate. Regarding the nucleation of α-Al, ΔT represents the disparity between the theoretical and experimental nucleation temperatures of α-Al. The CA-CCTA results indicate that the nucleation undercooling (ΔT) of Sr-free and Al-13.6Cu-6Si-0.3Sr alloys are 5.3 and 6.5 °C, respectively.

The increasing undercooling is provided by the constituent overcooling due to the high active Sr element. The growing decrease in temperature below the freezing point leads to an increase in the rate at which particles form in heterogeneous nucleation. In other words, the augmentation of undercooling aids in the nucleation of α-Al and leads to a finer grain size of α-Al. This conclusion aligns with the observed microstructure evolution (refer to Fig. 1 for further details).

The enlarged figure of the Al-Si structure can be seen in Fig. 4c, which is obtained from the solidification curves and first derivative curves. Significantly, the inclusion of Sr results in a remarkable decrease in the nucleation temperature of the Al-Si eutectic formation, plummeting from 543.6 to 533.8 °C. The estimated nucleation temperature of the Al-Si eutectic structure is roughly 546.7 °C. The temperature difference (ΔT) of the Al-Si eutectic formation rises significantly from 3.1 to 12.9 °C, resulting in the Si phase morphology in the eutectic structure breaking from coarse plate-like to small coral-like structures, with a more uniform and dispersed distribution (refer to Fig. 3(a-d) for more information). It should be emphasized that the temperature at which the Sr-free alloy reaches the
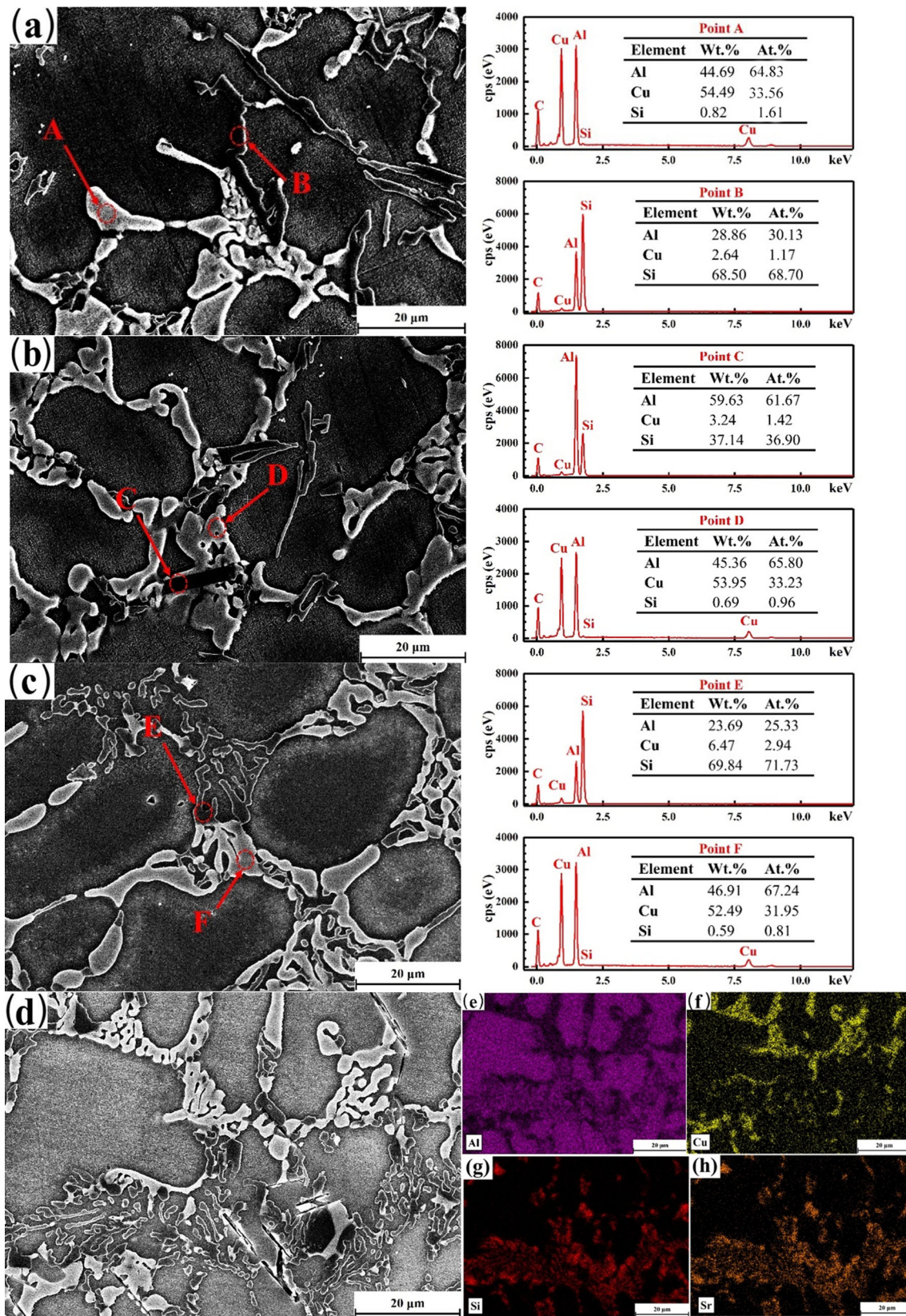
Fig. 3 SEM images and corresponding EDS analysis at various points of the as-cast alloys: (a) Al-13.6Cu-6Si, (b) Al-13.6Cu-6Si-0.1Sr, (c) Al-13.6Cu-6Si-0.3Sr, as well as EDS mappings of (d) as-cast Al-13.6Cu-6Si-0.5Sr, (e-h) Al, Cu, Si, Sr element mapping image, respectively
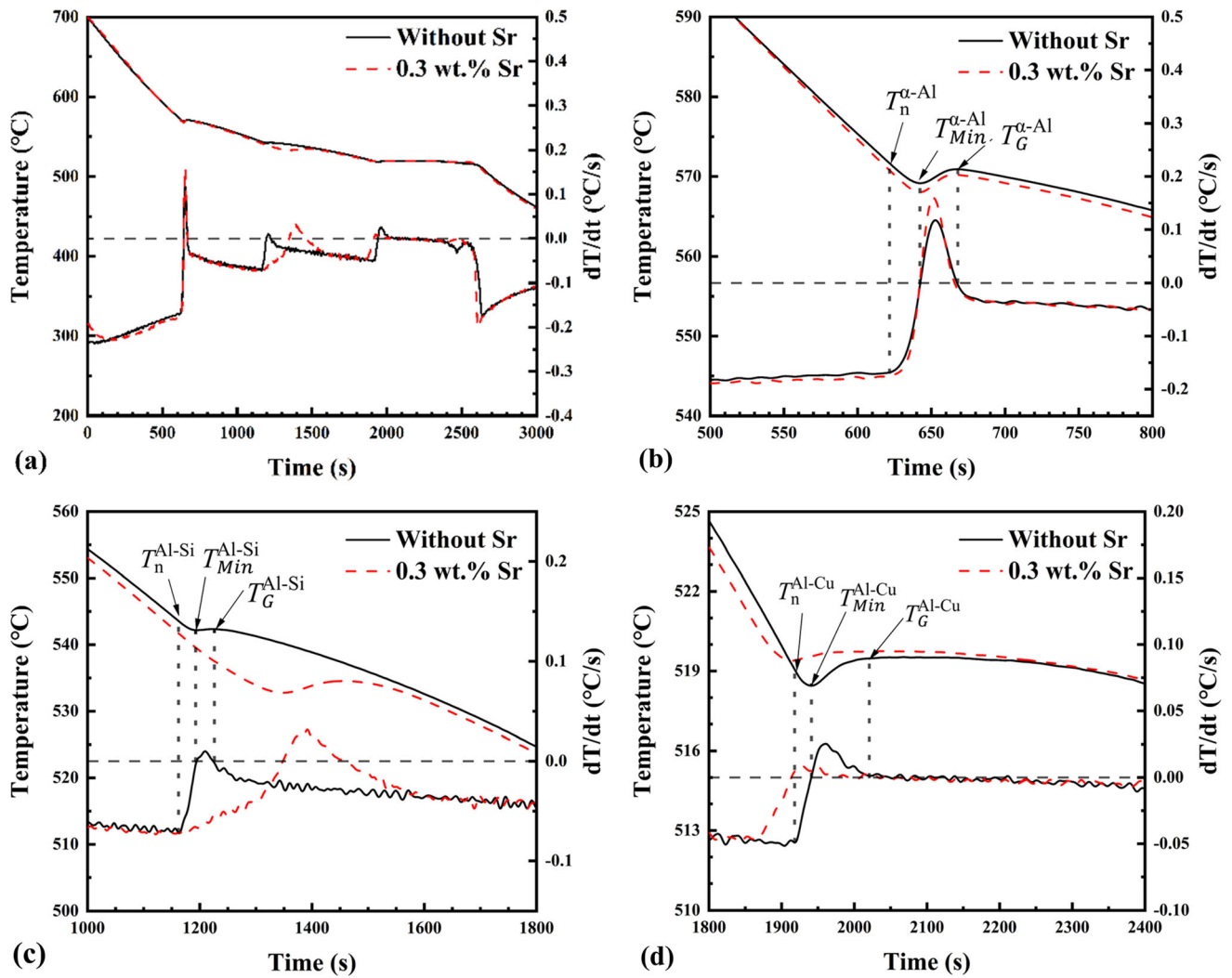
Fig. 4 (a) The solidification curves of Al-13.6Cu-6Si and Al-13.6Cu-6Si-0.3Sr melts, (b) the enlarge figure of α-Al, (c) the enlarge figure of Al-Si eutectic structure, and (d) the enlarge figure of Al-Al₂Cu eutectic structure

Table 2 List of the solidification characteristic parameters identified during solidification by CA-CCTA.

Symbol	Description
T_n^{a-Al}	Nucleation temperature of α-Al
T_{Min}^{a-Al}	Minimum nucleation temperature of α-Al
T_G^{a-Al}	Growth temperature of α-Al
T_n^{Al-Si}	Nucleation temperature of Al-Si eutectic structure
T_{Min}^{Al-Si}	Minimum nucleation temperature of Al-Si eutectic structure
T_G^{Al-Si}	Growth temperature of Al-Si eutectic structure
T_n^{Al-Cu}	Nucleation temperature of Al-Al₂Cu eutectic structure
T_{Min}^{Al-Cu}	Minimum nucleation temperature of Al-Al₂Cu eutectic structure
T_G^{Al-Cu}	Growth temperature of Al-Al₂Cu eutectic structure
T_s	Solidus temperature

T_G^{Al-Si} (Al-Si) value is 542.4 °C, significantly surpassing the corresponding value for the Al-13.6Cu-6Si-0.3Sr alloy. The main reason for the notable decrease in the growth temperature of the Al-Si eutectic structure is the absorption of the Sr element. Furthermore, there are no significant changes in the temperature of growth, the lowest temperature for nucleation, and the temperature of growth for the Al-Al₂Cu eutectic structure. The aforementioned observation suggests that the inclusion of Sr has negligible influence on the shape and arrangement of the Al₂Cu phase, aligning with the SEM findings depicted in Fig. 3.

3.2 Thermal Conductivity

The electrical and thermal conductivity of as-cast Al-13.6Cu-6Si-xSr alloys is depicted in Fig. 6. The related values are summarized in Table 4. According to the experimental results, it can be observed that the densities of these samples decrease in a linear manner as the Sr content increases. Meanwhile, the calculated heat capacities linearly decrease at the same time. It is noteworthy that the thermal diffusivities of Al-13.6Cu-6Si-xSr alloys firstly elevate from 0.392 ± 0.005 to 0.432 ± 0.005 cm²/s and then slightly decline to

Table 3 Solidification parameters of α-Al, Al-Si, and Al-Al$_2$Cu eutectic phases extracted from cooling curves (unit: °C).

	α-Al		Al-Si eutectic		Al-Al$_2$Cu eutectic	
	Withour Sr	0.3 wt.% Sr	Withour Sr	0.3 wt.% Sr	Withour Sr	0.3 wt.% Sr
T_n	571.6	570.4	543.6	533.8	519.4	520.1
T_{Min}	569.2	568.0	542.2	532.7	518.6	519.2
T_G	570.9	570.2	542.4	533.5	519.4	519.7
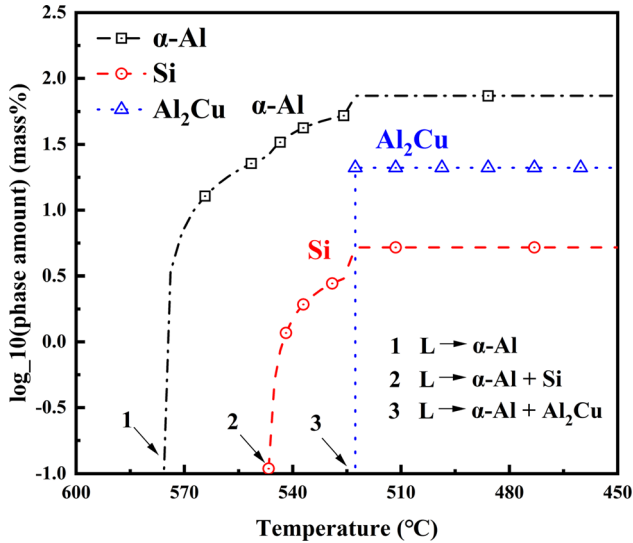
Fig. 5 Simulated solidification path of hypoeutectic Al-13.6Cu-6Si alloy predicted by JmatPro

Fig 6 The electrical and thermal conductivity of as-cast Al-13.6Cu-6Si alloys with different Sr contents

0.407 ± 0.003 cm^2/s. Al-13.6Cu-6Si-0.3Sr alloy shows the highest thermal diffusivity.

From the data presented in Fig. 6, it is evident that the variation in electrical conductivity mirrors that of thermal conductivity. According to Wiedemann–Franz law (namely, $\lambda/\sigma = L_0 T$,) the ratio between thermal conductivity and electrical conductivity can be regarded as a constant, where L_0 is constant (2.45×10^{-8}V^2 K^{-2}) and T represents the absolute temperature. With an increase in Sr content from 0 to 0.3%, the electrical and thermal conductivity experience a rise from 17.01 ± 0.23 MS/m and 118.2 ± 1.6 W/(m K) to 18.32 ± 0.33 MS/m and 130.1 ± 1.5 W/(m K), respectively. Nevertheless, as the Sr content rises to 0.5%, the electrical and thermal conductivities experience a gradual decline, reaching 17.65 ± 0.13 MS/m and 122.4 ± 1.0 W/(m·K), respectively. Therefore, it can be concluded that the Al-13.6Cu-6Si alloy containing 0.3% Sr exhibits excellent electrical and thermal conductivity.

Electrons and lattice waves are the main carriers of thermal energy transfer in the thermal conductivity process of metal materials. Therefore, the thermal conductivity of the Al alloy is considered to be the combination of the electronic and lattice components, with the electronic component having a dominant influence. The equality of relaxation times for heat and electron transport connects the electronic thermal conductivity to electrical conductivity through the Wiedemann–Franz law (Ref 38). The Mattissen-Flemming rule states that the electrical resistivity of alloys is primarily affected by solid solute atoms,
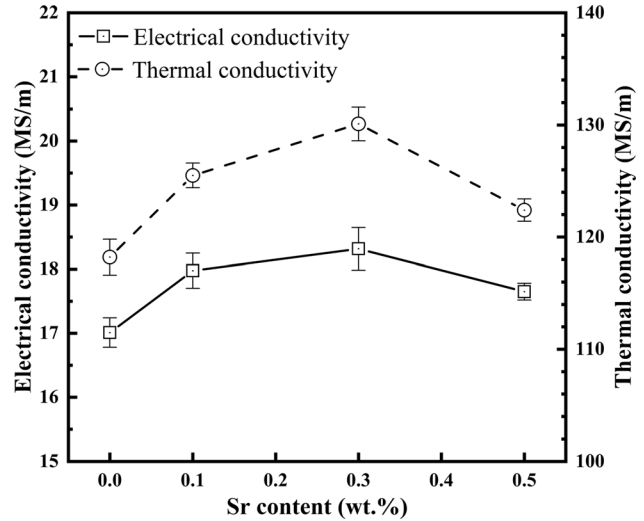
impurities, defects, and similar factors (Ref 34, 39). The corresponding expression is formulated as:

$$\rho = \rho^{Alpure} + \rho^{precipitates} + S_{GB}\Delta\rho^{GB} + L_{dislo}\Delta\rho^{dislo} + C_v\Delta\rho^{vac} + \sum_i C_{solu}^i \Delta\rho_{solu}^i$$

$$\text{(Eq 4)}$$

The value of ρ^{Alpure} is 2.665×10^{-8} Ω m. The term $\rho^{precipitates}$ refers to the resistivity caused by precipitates, which can be disregarded because the small Sr addition has minimal impact on the precipitates' volume fraction. The constants $\Delta\rho^{GB}$, $\Delta\rho^{dislo}$, $\Delta\rho^{vac}$, and $\Delta\rho_{solu}^i$ represent the effects of grain boundaries, dislocations, vacancies, and solid solute atoms on the electrical resistivity. The grain boundary fraction per unit volume is denoted as S_{GB}, while L_{dislo} represents the dislocation density. Additionally, C_v signifies the vacancy concentration, and C_{solu}^i indicates the concentration of solid solute atom i.

Based on the microstructure evolution shown in Fig. 3, the refinement of α-Al grains and the transformation of eutectic Si phase morphology lead to an increase in the S_{GB} value (the proportion of grain boundaries per unit volume), but this has minimal impact on the electrical resistivity of hypoeutectic Al-13.6Cu-6Si (Ref 40). Significantly, after the addition of 0.3% Sr, the Si phase underwent a remarkable morphological transformation, transitioning from a plate-like structure to a coral-like one. This change effectively broadened the pathways for electron movement, reducing the obstacles encountered during electron motion and decreasing the probability of

Table 4 The thermal diffusivity, density, heat capacity, and thermal conductivity of as-cast Al-13.6Cu-6Si alloys with different Sr contents

Alloy name	Property			
	Thermal diffusivity, cm²/s	Density, g/cm³	Heat capacity, J/(g K)	Thermal conductivity, W/(m K)
Al-13.6Cu-6Si	0.392 ± 0.005	3.525	0.8559	118.2 ± 1.6
Al-13.6Cu-6Si-0.1Sr	0.416 ± 0.003	3.524	0.8557	125.5 ± 1.1
Al-13.6Cu-6Si-0.3Sr	0.432 ± 0.005	3.524	0.8552	130.1 ± 1.5
Al-13.6Cu-6Si-0.5Sr	0.407 ± 0.003	3.522	0.8548	122.4 ± 1.0

electron scattering (as shown in Fig. 7). Additionally, it improves the interconnection among grains, consequently decreasing the dispersion of unbound electrons. Enhanced connectivity between the grains leads to a higher average distance traveled by conducting electrons, ultimately enhancing the thermal conductivity of the as-cast Al-13.6Cu-6Si from 118.2 to 130.1 W/(m K). Furthermore, the addition of Sr strategically reduces the Si solid solution in the α-Al matrix, as verified by wavelength dispersion spectrometer (WDS) analysis according to Wang et al. (Ref 36). The decrease in Si concentration in the α-Al matrix results in a reduction in lattice distortion, thereby enhancing the thermal conductivity of these alloys. However, when the Sr content reaches 0.5%, the thermal conductivity experiences a slight decrease to 122.4 W/(m K). This decline is partly attributed to the transformation of Si phase, and the reformation of block like Si phase reduces the connectivity between alloy grains, leading to an increase in obstacles encountered during electron movement. On the other hand, it is attributed to the increase in alloy porosity, which diminishes the effective heat transfer area during the thermal conduction process.

3.3 Mechanical Properties

In Fig. 8a, the engineering stress–strain curves of as-cast Al-13.6Cu-6Si-xSr alloys are shown, along with a small image showing a standard tensile test sample. Figure 8b displays the mechanical properties associated with these alloys. The Al-13.6Cu-6Si alloy, which is hypoeutectic, demonstrates outstanding tensile characteristics, showcasing a yield strength of approximately 150 ± 3.5 MPa and an ultimate tensile strength of around 270 ± 5.0 MPa. However, the ductility of this alloy is relatively poor, amounting to only 3.0 ± 0.25%. Simultaneously, the inclusion of Sr improves the alloy's strength and ductility. At a Sr content of 0.3%, the alloy attains its maximum ultimate tensile strength of 322 ± 6.2MPa and a 4.6 ± 0.2% elongation. In comparison with the original alloy, the enhancements in maximum tensile strength and elongation reach 20.8% and 53.3%, correspondingly. However, when the Sr content rises to 0.5%, the alloy experiences a notable decline in its mechanical characteristics. This includes a decrease in both ultimate tensile strength and elongation, which reach values of approximately 230 ± 4.8MPa and 2.2 ± 0.3%, respectively. These values are lower compared to the base alloy.

In this study, the comprehensive quality index Q is used to evaluate the comprehensive mechanical properties of materials. The Q value includes the strength and elongation is defined as follows:

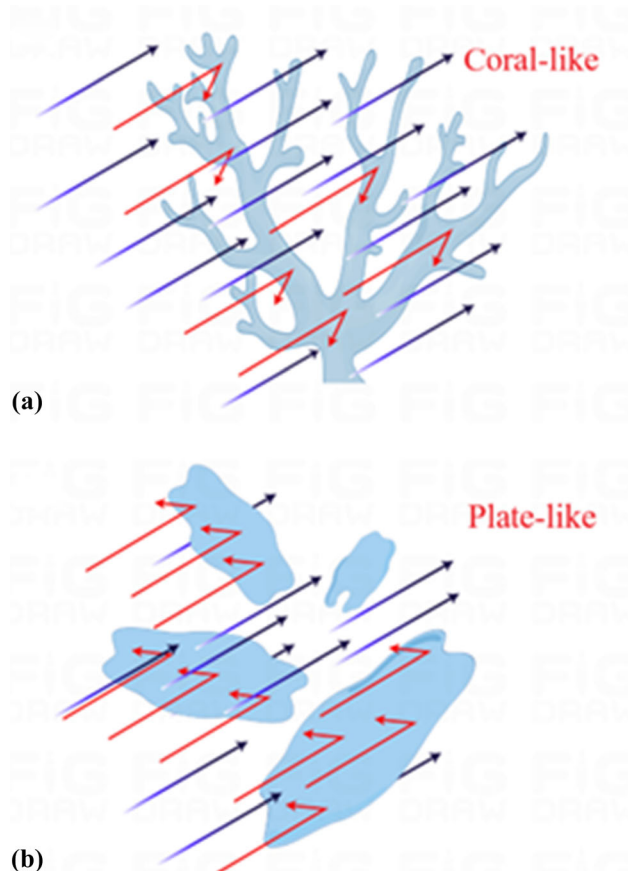$$Q = \text{UTS} + a \times \log(\text{elongation}\%) \qquad (\text{Eq 5})$$

(a) Coral-like

(b) Plate-like

Fig. 7 Schematic diagram of the influence of different eutectic Si phase morphologies on electron motion: (a) coral-like, (b) plate-like

where a is 150 MPa for aluminum alloys (Ref 41-44). The calculated results show that the Q value of Al-13.6Cu-6Si alloy is only 341.57 MPa. According to the given date, incorporating 0.3% Sr into the base alloy results in a notable rise in the Q value, peaking at 421.41 MPa, which is approximately 23.3% greater than the Q value of the base alloy. Nevertheless, the inclusion of additional Sr (specifically, 0.5%) leads to a notable reduction in the Q value, which drops to 281.36 MPa. This decrease in performance is likely due to the negative effect of excessive Sr content on the alloy's microstructure or mechanical properties.

Figure 9 shows the fracture surfaces of the Al-13.6Cu-6Si alloys with different levels of Sr addition. The point-scanning EDS (energy-dispersive spectroscopy) results, corresponding to the fracture surfaces spanning from Point A to Point F, are
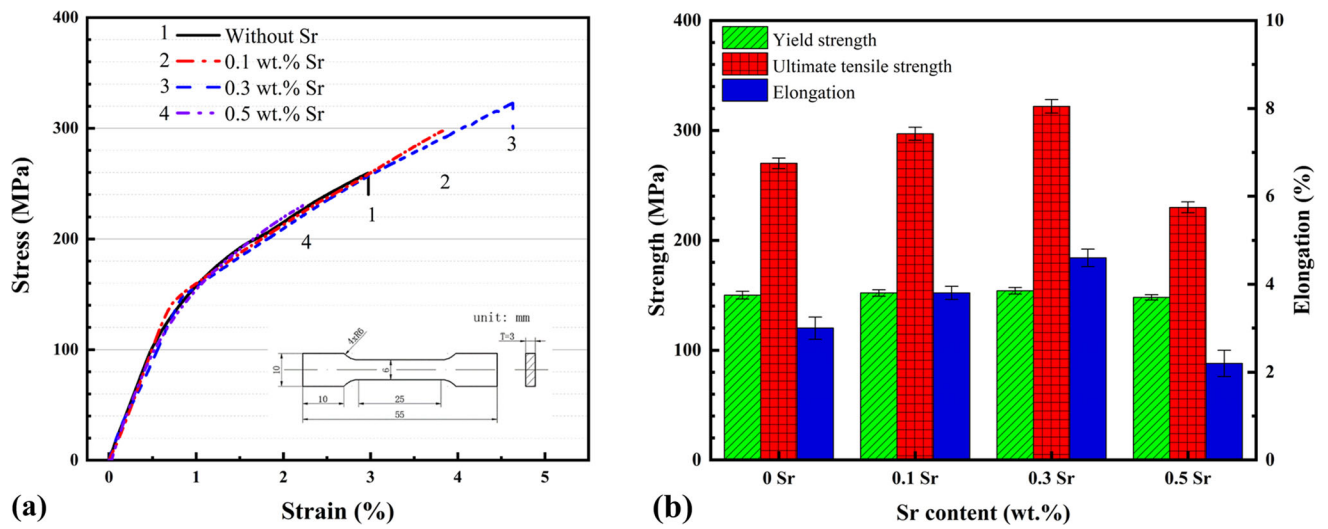
Fig. 8 (a) The tensile engineering stress–strain curves and (b) the corresponding mechanical properties of as-cast Al-13.6Cu-6Si alloys with different Sr contents
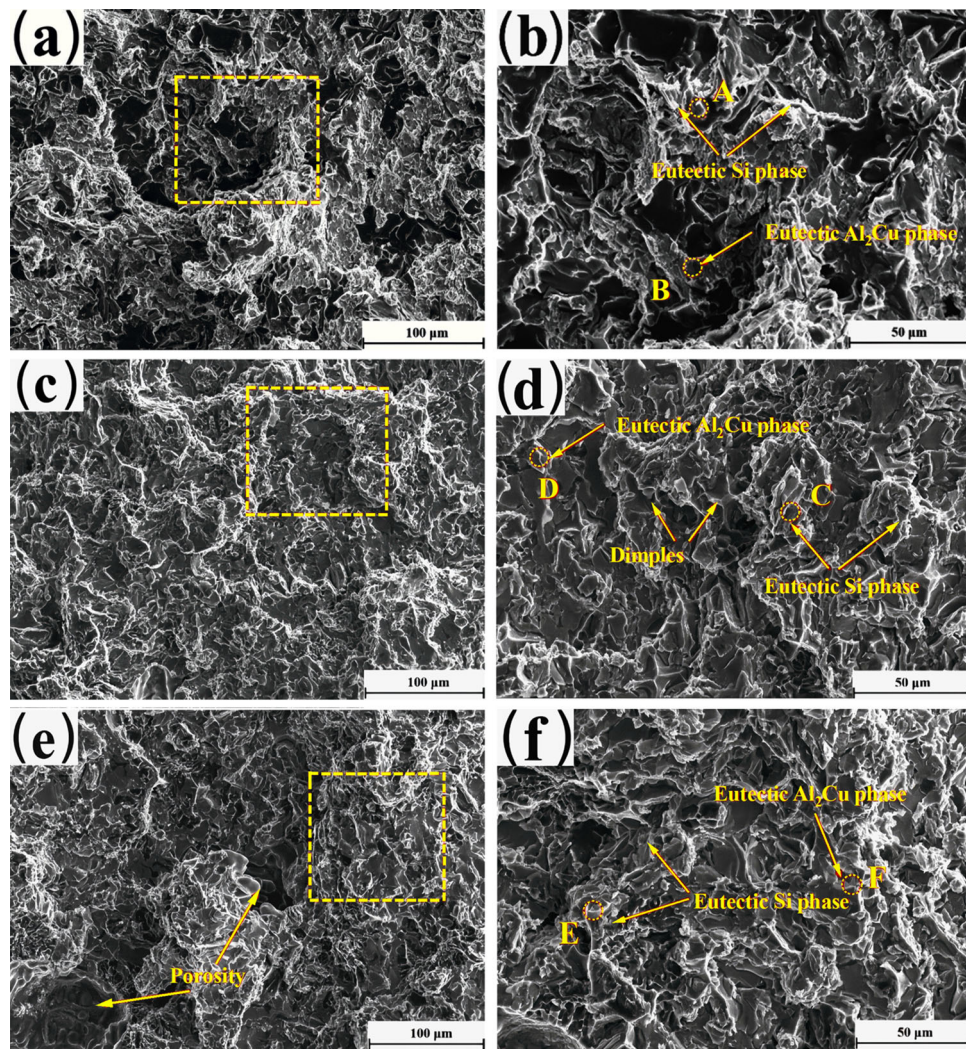

Fig. 9 The fracture surfaces of the hypoeutectic Al-13.6Cu-6Si alloys with various Sr addition levels: (a) and (b) 0 wt.%, (c) and (d) 0.3 wt.%, as well as (e) and (f) 0.5 wt.%
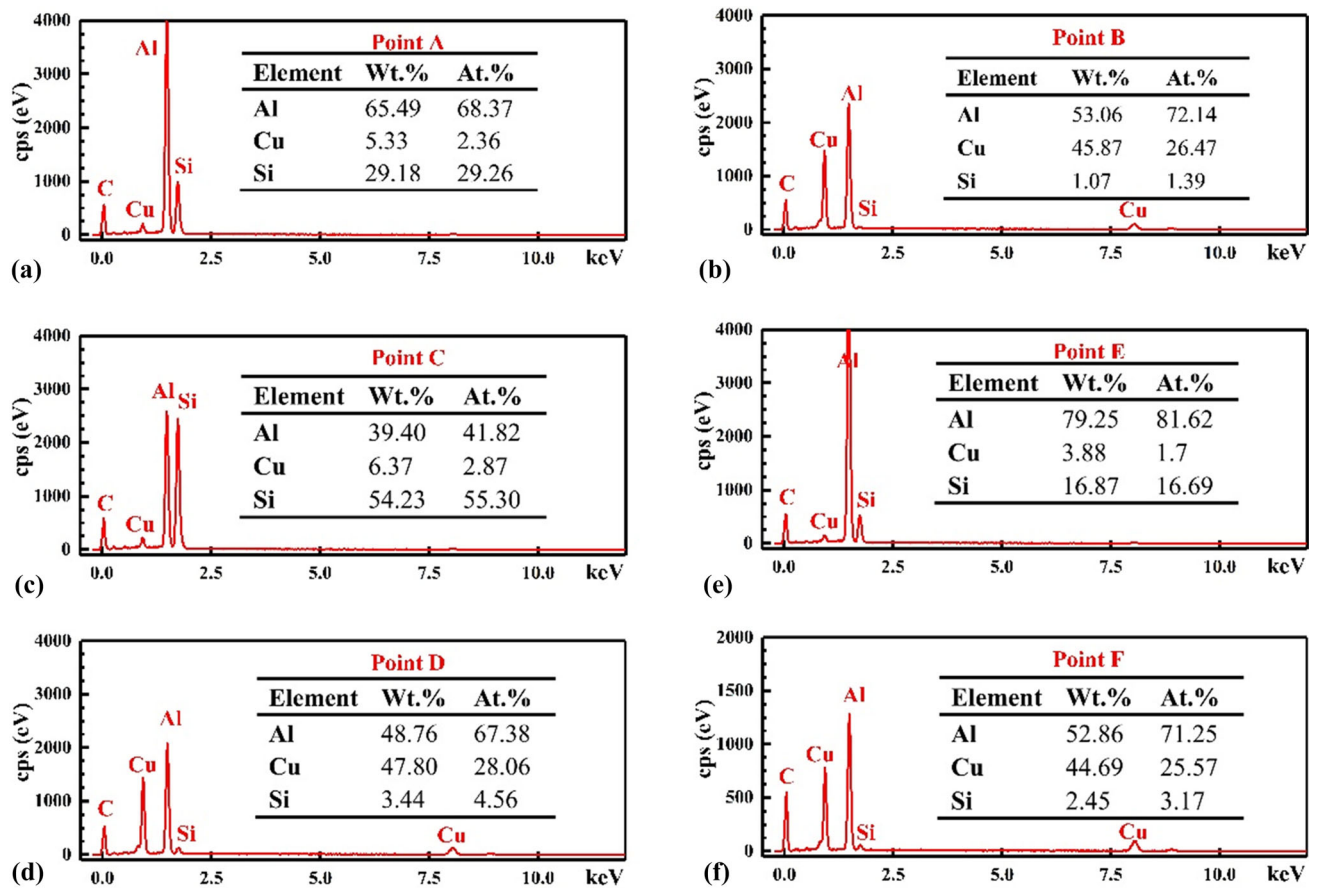
Fig. 10 The corresponding point-scanning EDS results of fracture surfaces: (a) Point A, (b) Point B, (c) Point C, (d) Point D, (e) Point E, (f) Point F

Point A

Element	Wt.%	At.%
Al	65.49	68.37
Cu	5.33	2.36
Si	29.18	29.26

Point B

Element	Wt.%	At.%
Al	53.06	72.14
Cu	45.87	26.47
Si	1.07	1.39

Point C

Element	Wt.%	At.%
Al	39.40	41.82
Cu	6.37	2.87
Si	54.23	55.30

Point E

Element	Wt.%	At.%
Al	79.25	81.62
Cu	3.88	1.7
Si	16.87	16.69

Point D

Element	Wt.%	At.%
Al	48.76	67.38
Cu	47.80	28.06
Si	3.44	4.56

Point F

Element	Wt.%	At.%
Al	52.86	71.25
Cu	44.69	25.57
Si	2.45	3.17

graphically represented in Fig. 10. From Fig. 9(a) and (b) ombination of typical cleavage fracture of α-Al and eutectic separation can be observed. The microstructure morphology of fracture surfaces exhibits rock candy shape. The above appearance suggests that the Al-13.6Cu-6Si is brittle, which is in agreement with the tensile results. The based alloy presents poor ductility. Furthermore, the eutectic Si and Al$_2$Cu phases are observed to align along the phase boundaries, forming a contiguous network structure. The arrangement of this network is not conducive to the tensile characteristics of the underlying alloy. However, the introduction of the Sr element results in a transformation of the fracture mechanism. In particular, the Al-13.6Cu-6Si-0.3Sr alloy displays a limited number of dimple ruptures within the α-Al regions, which aids in improving its ductility. These details can be observed in Fig. 9d. The tensile results also indicate a notable elongation to failure in Al-13.6Cu-6Si alloy with 0.3% Sr addition.

When the Sr content rises to 0.5%, porosities start to appear on the surfaces subjected to tension. The α-Al in the porosity regions exhibits a dendritic shape, indicating the formation of more gas holes during the solidification process due to the excessive addition of Sr. According to reports, Sr is an element with high activity that improves the absorption of gas in the molten alloy (Ref 45). The enhanced gas absorption diminishes the Sr alteration and facilitates the creation of gas voids, ultimately leading to a substantial reduction in tensile characteristics.

4. Conclusions

This study delves into the influence of Sr addition on the microstructures, thermal conductivities, and mechanical properties of hypoeutectic Al-13.6Cu-6Si alloys, shedding light on the effect mechanisms of the alkaline-earth element Sr. The main findings are as follows:

1. The inclusion of Sr improves the α-Al dendrites in hypoeutectic Al-13.6Cu-6Si alloys, converting the eutectic Si phase from a plate-like structure to a delicate and consistent coral-like form. Moreover, the inclusion of Sr has a negligible effect on the structure and dispersion of the Al$_2$Cu phase.
2. The incorporation of small amounts of Sr leads to concurrent enhancements in the tensile properties and thermal conductivity of Al-Cu-Si alloys. The improvements in strength, plasticity, and thermal conductivity can be primarily attributed to the grain refinement and modification of the Si phase.
3. The presence of Sr elements causes extra cooling within the components, resulting in a higher rate of nucleation for heterogeneous nucleation and a reduction in the size of α-Al grains.
4. The alloy treated with 0.3% Sr exhibits a thermal conductivity of 130.1 W/(m·K), an ultimate tensile strength of 322 MPa, and an elongation of 4.6%. Compared to the hypoeutectic Al-13.6Cu-6Si, these

properties are improved by 10%, 19%, and 53%, respectively.

Conflict of interest

The authors assert that there is no conflict of interest.

References

1. K. Chanyathunyaroj, U. Patakham, S. Kou, and C. Limmaneevichitr, Mechanical Properties of Squeeze-Cast Al-7Si-0.3Mg Alloys with Sc-Modified Fe-Rich Intermetallic Compounds, *Rare Met.*, 2018, **37**(9), p 769–777

2. M.F. Qi, Y.L. Kang, J.Y. Li, and B. Shang, Improvement in Mechanical, Thermal Conductivity and Corrosion Performances of a New High-Thermally Conductive Al-Si-Fe Alloy through a Novel R-Hpdc Process, *J. Mater. Process. Technol.*, 2020, **279**, p 116586

3. E. Vandersluis, P. Emadi, B. Andilab, and C. Ravindran, The Role of Silicon Morphology in the Electrical Conductivity and Mechanical Properties of As-Cast B319 Aluminum Alloy, *Metall. Mater. Trans. A*, 2020, **51**(4), p 1874–1886

4. X. Cui, H. Cui, Y. Wu, and X. Liu, The Improvement of Electrical Conductivity of Hypoeutectic Al-Si Alloys Achieved by Composite Melt Treatment, *J. Alloys Compd.*, 2019, **788**, p 1322–1328

5. G. Luo, X. Zhou, C.B. Li, Z. Huang, and J. Du, A Quantitative Study On the Interaction Between Silicon Content and Heat Treatment On Thermal Conductivity of Al-Si Binary Alloys, *Int. J. Met.*, 2022, **16**(3), p 1585–1594

6. P. Tang, S. Lu, H. Chen, F. Mo, and J. Li, Effect of Cerium Addition On Microstructure, Thermal and Rheological Properties of Hypoeutectic Al-Ni Alloy, *Mater. Today Commun.*, 2023, **36**, p 106842

7. C. Tao, X.N. Cheng, Z.Q. Li, G.L. Liu, F.H. Xu, S.K. Xie, Z.H. Kuang, Y. Guo, and H.X. Liu, Mechanism of Cryogenic, Solid Solution and Aging Compound Heat Treatment of Die-Cast Al Alloys Considering Microstructure Variation, *Rare Met.*, 2023, **42**(9), p 3130–3138

8. P. Tang, J.S. Lu, Y.X. Yang, and W.Y. He, Microstructure and Mechanical Properties of Cast Al-15Mg2Si-8Si-Based Alloy with Various Cr-Sb Ratio Addition, *J. Mater. Eng. Perform.*, 2023, **5**, p 1–5

9. V.A. Aranda, I.A. Figueroa, G. González, J.A. García-Hinojosa, and I. Alfonso, Study of the Microstructure and Mechanical Properties of Al-Si-Fe with Additions of Chromium by Suction Casting, *J. Alloys Compd.*, 2021, **853**, p 157155

10. P. Tang, Z. Hu, Y. Zhao, and Q. Huang, Investigation on the Solidification Course of Al-Si Alloys by Using a Numerical Newtonian Thermal Analysis Method, *Mater. Res. Express*, 2017, **4**(12), p 126511

11. S.P. Xu, C.S. Shi, N.Q. Zhao, and C.N. He, Microstructure and Tensile Properties of A356 Alloy with Different Sc/Zr Additions, *Rare Met.*, 2021, **40**(9), p 2514–2522

12. X. Yan, X.J. Xu, Q.S. Zhou, and Z.W. Sun, Effect of Solid Solution System On the Properties of Al-6.5Si-5.5Cu-0.2Zr-0.01Sr-0.06Ti-0.2Ce Alloy in the Aging State, *J. Mater. Eng. Perform.*, 2023, **15**, p 15

13. P. Tang, Q. Liu, F. Yu, F. Mo, and L. Qin, Effect and its Mechanism of Fixed-Ratio and Incremented 3Be-Sb Complex Modifier On Microstructures and Properties of Hypereutectic Al-Si-Mg Alloy, *J. Alloys Compd.*, 2023, **931**, p 167478

14. H.X. Lu, Q. Zhu, S.P. Midson, W.Y. Qu, F. Zhang, and D.Q. Li, Forming Conditions of Blisters During Solution Heat Treatment of Al-Si Alloy Semi-Solid Die Castings, *Rare Met.*, 2023, **42**(11), p 3851–3858

15. Y.H. Cho, H.W. Kim, J.M. Lee, and M.S. Kim, A New Approach to the Design of a Low Si-Added Al-Si Casting Alloy for Optimising Thermal Conductivity and Fluidity, *J. Mater. Sci.*, 2015, **50**(22), p 7271–7281

16. C. Wen, J. Gan, C. Li, Y. Huang, and J. Du, Comparative Study On Relationship Between Modification of Si Phase and Thermal Conductivity of Al-7Si Alloy Modified by Sr/Re/B/Sb Elements, *Int. J. Met.*, 2021, **15**(1), p 194–205

17. W.P. Li, Y.L. Zhang, and J. Mao, Enhanced Strength and Electrical Conductivity of Al-03Ce Alloy Simultaneously with Ti(C, N) Nanoparticle Addition, *Rare Met.*, 2021, **40**(7), p 1890–1896

18. G. Gouveia, L. Gomes, N. Cheung, A. Garcia, and J. Spinelli, Mechanical Properties, Microstructural Features and Correlations with Solidification Rates of Al-Cu-Si Ultrafine Eutectic Alloys, *Adv. Eng. Mater.*, 2020, **23**, p 2001177

19. Q. Cai, C.L. Mendis, I.T.H. Chang, and Z. Fan, Microstructure and Mechanical Properties of New Die-Cast Quaternary Al-Cu-Si-Mg Alloys, *Mater. Sci. Eng. A*, 2021, **800**, p 140357

20. B.K. Kang and I. Sohn, Effects of Cu and Si Contents on the Fluidity, Hot Tearing, and Mechanical Properties of Al-Cu-Si Alloys, *Metall. Mater. Trans. A*, 2018, **49**(10), p 5137–5145

21. G.L. de Gouveia, R. Kakitani, L.F. Gomes, C.R.M. Afonso, N. Cheung, and J.E. Spinelli, Slow and Rapid Cooling of Al-Cu-Si Ultrafine Eutectic Composites: Interplay of Cooling Rate and Microstructure in Mechanical Properties, *J. Mater. Res.*, 2019, **34**(8), p 1381–1394

22. Y.D. Sui, L.N. Han, and Q.D. Wang, Effects of Thermal Exposure on the Microstructure and Mechanical Properties of Al-Si-Cu-Ni-Mg-Gd Alloy, *J. Mater. Eng. Perform.*, 2019, **28**(2), p 908–915

23. X.M. Pan, C. Lin, H.D. Brody, and J.E. Morral, An Assessment of Thermodynamic Data for the Liquid Phase in the Al-Rich Corner of the Al-Cu-Si System and its Application to the Solidification of A319 Alloy, *J. Phase Equilib. Diffus.*, 2005, **26**(3), p 225–233

24. J. Campbell, The Fluidity of Al-Cu-Si Alloys-a Discussion of the Paper by Garbellini, Palacio and Biloni (1990), *Cast Metals*, 1991, **4**(2), p 101–102

25. G.S. Peng, X.Y. Fu, Y.C. Gu, G.S. Song, S.S. Chen, Q.Q. Sun, and W.D. Hua, Microstructural Evolution and Strengthening Behavior of High-Pressure Die-Cast High-Cu Al-Si-Cu-Mg Alloy with T5 Treatment, *J. Mater. Eng. Perform.*, 2022, **31**(7), p 5432–5440

26. E. Vandersluis, C. Ravindran, D. Sediako, A. Elsayed, and G. Byczynski, Strontium-Modification in the Stepwise Solidification of A319 Al Alloy: An in-Situ Neutron Diffraction Study, *J. Alloys Compd.*, 2019, **792**, p 240–249

27. C. Xu, F. Wang, H. Mudassar, C. Wang, S. Hanada, W. Xiao, and C. Ma, Effect of Sc and Sr on the Eutectic Si Morphology and Tensile Properties of Al-Si-Mg Alloy, *J. Mater. Eng. Perform.*, 2017, **26**(4), p 1605–1613

28. X.L. Zhang, J.H. Liu, W.S. Li, H.T. Zhou, and S.C. Wang, Effect of Sr-Ce Modification on the Microstructure and Mechanical Properties of A356 Alloy, *Int. J. Met.*, 2023, **17**(2), p 1008–1020

29. X. Du, F. Zhao, C. Peng, D. Zhu, K. Li, Y. Wan, Y. Tan, and R. Yang, Effect of Sr on the Microstructure and Properties of Al-6.5Si-20Cu-1.5Ni Filler Metal for Brazing 6063 Aluminum Alloy, *Weld. World*, 2023, **67**(8), p 2039–2048

30. P. Tang, J. Lu, Y. Yang, F. Mo, and L. Wei, Effect of Various Er/Al-Ti-C Ratios on Microstructure and Tensile Properties of the As-Cast Al-10Si-0.8Fe Alloy, *J. Alloys Compd.*, 2023, **968**, p 172237

31. Y. Wang, P.Y. Chen, Y.H. Lin, M. Zhao, and C.D. Li, An Al-12Si/Zns Powder Inoculant for Eutectic Silicon in Al-12Si Alloy, *China Found.*, 2022, **19**(2), p 149–157

32. A. Rudajevová, F. von Buch, and B.L. Mordike, Thermal Diffusivity and Thermal Conductivity of Mgsc Alloys, *J. Alloys Compd.*, 1999, **292**(1), p 27–30

33. G. Luo, Y. Huang, C. Li, Z. Huang, and J. Du, Microstructures and Mechanical Properties of Al-2Fe-xCo Ternary Alloys with High Thermal Conductivity, *Materials*, 2020, **13**, p 3728

34. P. Pan, B. Jiang, Y. Guo, Y. Wang, H. Xu, and M. Hu, Effect of Cryorolling on Microstructure, Conductivities, and Mechanical Properties of a Cast Near-Eutectic Al-Si-Fe-Mg Alloy, *J. Mater. Eng. Perform.*, 2023. https://doi.org/10.1007/s11665-023-08931-0

35. J. Li, M. Albu, F. Hofer, and P. Schumacher, Solute Adsorption and Entrapment During Eutectic Si Growth in A-Si-Based Alloys, *Acta Mater.*, 2015, **83**, p 187–202

36. K. Wang, W. Li, W. Xu, S. Hou, and S. Hu, Simultaneous Improvement of Thermal Conductivity and Strength for Commercial a356 Alloy Using Strontium Modification Process, *Met. Mater. Int.*, 2021, **27**(11), p 4742–4756

37. J. Barrirero, M. Engstler, N. Ghafoor, N. de Jonge, M. Odén, and F. Mücklich, Comparison of Segregations Formed in Unmodified and Sr-Modified Al-Si Alloys Studied by Atom Probe Tomography and Transmission Electron Microscopy, *J. Alloys Compd.*, 2014, **611**, p 410–421

38. H.C. Pan, F.S. Pan, R.M. Yang, J. Peng, C.Y. Zhao, J. She, Z.Y. Gao, and A. Tang, Thermal and Electrical Conductivity of Binary Magnesium Alloys, *J. Mater. Sci.*, 2014, **49**(8), p 3107–3124

39. X. Sauvage, E.V. Bobruk, M.Y. Murashkin, Y. Nasedkina, N.A. Enikeev, and R.Z. Valiev, Optimization of Electrical Conductivity and Strength Combination by Structure Design at the Nanoscale in Al-Mg-Si Alloys, *Acta Mater.*, 2015, **98**, p 355–366

40. H.X. Jiang, S.X. Li, Q.J. Zheng, L.L. Zhang, J. He, Y. Song, C.K. Deng, and J.Z. Zhao, Effect of Minor Lanthanum on the Microstructures, Tensile and Electrical Properties of Al-Fe Alloys, *Mater. Des.*, 2020, **195**, p 108991

41. C.R. Qiu, S.N. Miao, X.R. Li, X.C. Xia, J. Ding, Y.N. Wang, and W.M. Zhao, Synergistic Effect of Sr and La on the Microstructure and Mechanical Properties of A356.2 Alloy, *Mater. Des.*, 2017, **114**, p 563–571

42. Z.M. Shi, Q. Wang, G. Zhao, and R.Y. Zhang, Effects of Erbium Modification on the Microstructure and Mechanical Properties of A356 Aluminum Alloys, *Mater. Sci. Eng. A*, 2015, **626**, p 102–107

43. S.P. Nikanorov, V.N. Osipov, and L.I. Regel, Structural and Mechanical Properties of Directionally Solidified Al-Si Alloys, *J. Mater. Eng. Perform.*, 2019, **28**(12), p 7302–7323

44. M. Tocci, R. Donnini, G. Angella, E. Gariboldi, and A. Pola, Tensile Properties of a Cast Al-Si-Mg Alloy with Reduced Si Content and Cr Addition at High Temperature, *J. Mater. Eng. Perform.*, 2019, **28**(11), p 7097–7108

45. M.R.S. Ganesh, N. Reghunath, M.J. Levin, A. Prasad, S. Doondi, and K.V. Shankar, Strontium in Al-Si-Mg Alloy: A Review, *Met. Mater. Int.*, 2022, **28**(1), p 1–40